

# Frequency Selective Surface with Arbitrary Shapes and Its Application to Filter Design

Maurice Sesay<sup>1,2</sup>, Xin Jin<sup>1</sup>, and Zhengbiao Ouyang<sup>1,\*</sup>

**Abstract**—Investigation on dielectric frequency selective structure with arbitrary shaped grating is done numerically for filter applications. To obtain well designed parameters, the effects of shape, size and dielectric constant of the structure are carefully studied. We examine in detail various structures and their spectral response which have not been reported by other authors. It is also shown how the frequency selective behavior of the structure can be controlled to meet a specific purpose for narrow linewidth filtering for normal incident angle. Results obtained for the scattering of several dielectric frequency selective surfaces are compared with both theoretical and experimental results presented in literatures, showing very good agreement. The effect of arbitrary angle of incidence is also shown to excite higher order Floquet modes that affect the filtering properties.

## 1. INTRODUCTION

A dielectric grating is an array of dielectric material having a periodic variation in refraction index. The analysis of the electromagnetic behavior of such structures has been the subject of various studies. Moreover, a variety of devices used in the microwave and optical frequency bands, such as frequency-selective filters and polarization filters, have been proposed [1–4]. The sidebands of the filter can be made arbitrarily low over a large frequency range by adding layers with dielectric constants and thicknesses satisfying antireflection (AR) and high-reflection (HR) conditions [3]. Furthermore, periodic array structures also have many applications in antennas and waveguides for bandwidth enhancement or dual-band operations [5].

Various numerical methods have been used to investigate the scattering problem. When the scatterer is a circular cylinder or sphere, the eigenfunction expansion method can be used. On the other hand, numerical techniques such as the finite element method [6], differential method [7] and domain methods [8, 9] have to be used for gratings in arbitrary shapes and complex structures. Furthermore, a numerical method based on a novel full wave vector-modal method [10, 11] for studying guidance and scattering by all-dielectric-guiding periodic structures has been presented, which has been applied to the accurate analysis of the modal spectrum, propagation constants and fields distribution of dielectric periodic structures for both TE and TM polarizations. Recently, modified dielectric frequency selective surfaces (MDFSS) have been proposed in [12]. In the MDFSS, the medium of higher constant named as core is unchanged, while the other medium, named as “cladding”, is substituted with a proper number of dielectric sub-gratings. Through cascading MDFSSs, enlarged bandwidth and angular stability have been demonstrated for stop-band filters [13]. However, some unique shapes of gratings and structures for filter design have not been studied in detail by most of these authors.

We focus our attention on filter properties of structures that have unique shapes with reduced edges in the case of squares. Furthermore, we present ways of controlling the spectral properties for these structures.

---

*Received 2 October 2013, Accepted 18 November 2013, Scheduled 23 November 2013*

\* Corresponding author: Zhengbiao Ouyang (zbouyang@szu.edu.cn).

<sup>1</sup> College of Electronic Science and Technology, THz Technical Research Center, Shenzhen University, Shenzhen 518060, China.

<sup>2</sup> Department of Electrical and Electronics Engineering, Fourah Bay College, University of Sierra Leone, Sierra Leone.

In this paper, we present detailed examinations on the design of filters for microwave applications using the numerical method based on volume integral equation [14] and method of moments (MoM) [15] with point matching. These methods are general and can be applied to a range of scattering problems including dielectric inhomogeneous materials. The structures considered in this paper does not require the rigorous coupled-wave theory used in [16, 17] to obtain the unique results. The scattering parameters of a one-dimensional (1-D) dielectric frequency selective structure (FSS) formed by one or two dielectric slabs with circular or deformed cylinders known as apertures within a unit cell are investigated. The motivation to carry such an investigation is to study how multiple scattering between objects can be used to control the filter properties. Controlling the resonance peak and bandwidth properties of the structure is of great priority in filter design and is highlighted in this paper without using complex design methodology or structures presented by other authors. Practically available dielectric materials are used in the investigation for proper choice of filter parameters. Numerical examinations of a dielectric frequency selective structure (DFSS) with two arbitrary shaped cylinders are considered. Unique spectral properties are obtained, of which we firstly investigated various parameters by brute-optimization method with single element per unit cell. This technique enables us to know which parameter plays a dominant effect on the spectral property. We then used the optimized parameters for our required filter design. As a further investigation, we considered the effect of arbitrary incident angle of waves to the structure. The incident angle consideration shows that higher Floquet modes are excited, and these modes affect the spectral properties of the filter. In this paper, we are also able to design narrow-linewidth filters.

## 2. METHODOLOGY AND FORMULATION

A two-dimensional grating composed of an array of uniformly spaced and identically shaped objects is arranged in the  $x$  direction with periodicity  $d$  as shown in Fig. 1. The incident field is a plane wave that is polarized in the  $z$  direction, which corresponds to a TM polarization in our case. The periodic structure is immersed in free space which separates the medium into two regions: region *I*, the homogeneous free space, and region *II*. The grating consists of cylinders with an arbitrary deformed shape. The total electric field  $\mathbf{E}(\mathbf{r})$  in region *I* is the superposition of the incident field  $\mathbf{E}^i(\mathbf{r})$  and the scattered field from the periodic structure expressed in terms of Floquet theorem as follows [14]:

$$\mathbf{E}(\mathbf{r}) = \mathbf{E}^i(\mathbf{r}) - \frac{1}{4} j k_0^2 \sum_{l=-\infty}^{\infty} \int_{S_0} H_0^{(2)}(k_0 \rho_l) \mathbf{E}(\mathbf{r}_0) \exp(-k_x l d) (\varepsilon_r(r_0) - 1) ds_0 \quad (1)$$

In Eq. (1),  $k_0$  is the wave number in region *I*, defined as  $k_0^2 = \omega^2 \mu_0 \varepsilon_0$  where  $\varepsilon_0$  and  $\mu_0$  are the free space dielectric and permeability constants respectively; the time variation factor  $\exp(j\omega t)$  is suppressed. The incident electric field  $\mathbf{E}^i(\mathbf{r})$  is propagating in region *I* with its  $\mathbf{k}$  vector on the  $x$ - $y$  plane at an angle  $\theta_i$  with respect to the  $y$  axis and  $\mathbf{r}$  is the position vector. The wave vector is given by  $\mathbf{k} = \hat{x}k_x + \hat{y}k_y$  where  $k_x = -k_0 \sin \theta_i$  and  $k_y = k_0 \cos \theta_i$  are the wave constants in the  $x$  and  $y$  directions, respectively.  $S_0$  is the surface cross sectional domain in the reference region *II* which consists of the unit cell where the integration is performed.  $\varepsilon_r$  is the inhomogeneous relative dielectric constant of the cylinders in

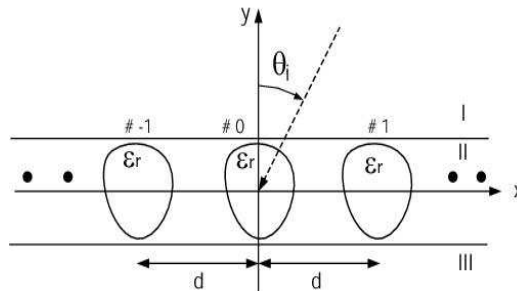


**Figure 1.** Geometry for a single layered grating with arbitrary shaped cylinders.

the region *II*.  $H_0^{(2)}$  is the zeroth-order Hankel function of the second kind.  $\rho_l$  is the distance between the observation point  $\mathbf{r}$  and the source point  $\mathbf{r}_0$  of the zeroth-order cylinder. To obtain the matrix equations for Eq. (1) by MoM, the pulse function is used as the basic function with a point matching technique. The reference region is divided into  $N$  number of cells, and the total electric field  $\mathbf{E}(\mathbf{r})$  and relative dielectric constants are assumed to be constant on each cell in the reference region. After several manipulations, the matrix equation is obtained as follows:

$$\sum_{n=1}^N C_{mn} E_n = E_m^i \quad (2)$$

where the matrix coefficient  $C_{mn}$  is given in reference [14].  $E_n$  is the total electric field at cell  $n$  and  $E_m^i$  the incidence field at cell  $m$ . The total unknown  $E_n$  can be solved by the GMRES (generalized minimum residual) solver. The matrix coefficients can be solved by the use of lattice sum techniques [18] and Poisson sum transformation [19]. With the total electric field obtained, the scattered fields radiating outwardly above and below the grating structure can be expressed as follows:

$$E_s^r = \sum_{l=-\infty}^{\infty} b_l^+ \exp[-jk_{xl}x - \kappa(k_{xl})y] \quad (3)$$

$$E_s^t = \sum_{l=-\infty}^{\infty} b_l^- \exp[-jk_{xl}x + \kappa(k_{xl})y] \quad (4)$$

where,

$$b_l^\pm = -j\pi/2 \sum_{n=1}^N E_n [\varepsilon_r(n) - 1] k_0 a_n J_1(k_0 a_n) \frac{1}{\kappa(k_{xl})} \exp[+jk_{xl}x_n \pm j\kappa(k_{xl})y_n] \quad (5)$$

$$k_{xl} = k_{x0} + ld \quad (6)$$

$$\kappa(k_{xl}) = (k_0^2 - k_{xl}^2)^{1/2} \quad (7)$$

and  $k_{xl}$  is the Floquet wave constant in  $x$  direction. The Floquet modes radiating above the grating represent the reflected field with Floquet mode amplitudes  $b_l^+$  and the modes radiating below the grating represent the transmitted field with Floquet mode amplitudes  $b_l^-$ . These modes constitute both propagating and evanescent modes in the homogeneous regions and the respective amplitude coefficients are obtained in [14]. The reflectance and transmittance from the grating structure are given by:

$$|R_l|^2 = |b_l^+|^2 \frac{\text{Re}[\kappa(k_{xl})]}{k_0 \cos \theta_{inc}} \quad (8)$$

$$|T_l|^2 = |\delta_{0l} + b_l^-|^2 \frac{\text{Re}[\kappa(k_{xl})]}{k_0 \cos \theta_{inc}} \quad (9)$$

where  $\text{Re}[\kappa(k_{xl})]$  is the real part of the propagating wave constant in  $y$  direction.

### 3. NUMERICAL CONSIDERATIONS

Numerical calculations are carried out for detailed examination of the scattering properties for various shaped structures including two scattering elements array. The results are shown for the frequency range that satisfied the condition  $d/\lambda < 1$ . For normal incident angle, only the fundamental Floquet mode  $l = 0$  is propagating in this range, thus the characteristics are plotted for the reflectance as a function of normalized wavelength, denoting the power reflection coefficient  $|R_0|^2$  of the fundamental space harmonic. The size of the aperture is appropriately chosen to be less than the free space wavelength so as to avoid higher order propagation that might leads to various problems like Wood's abnormality. We also analyzed for the case of an arbitrary incident angle and realized that higher order modes are excited. The propagation of the higher order modes together with the zeroth-order mode is not good for filter operation because it destroys the spectral properties of the filter. Before carrying out our design in detail, we firstly validate our data by comparing with the numerical results by other authors.

### 3.1. Numerical Results Validation

In order to compare our results with those of previous studies, the periodic grating in Fig. 2 consisting of two dielectric slabs in a period is considered. The grating thickness  $h$  is chosen to be half-wavelength for the central wavelength of the filters, so the spectral response shows a reduced reflectance around this wavelength. However, a simple reflection filter with a single-layer waveguide grating has been designed for a normal TM-polarized incident wave, whose reflectance property is shown in Fig. 3.

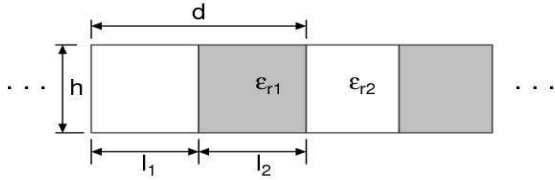


**Figure 2.** Model of a rectangular grating denoting grating period by  $d$ , width by  $l_1$  and  $l_2$ , layer thickness by  $h$  and relative dielectric constants by  $\epsilon_{r1}$  and  $\epsilon_{r2}$ .

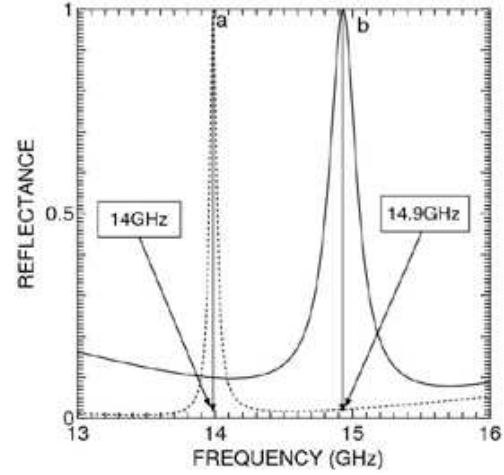


**Figure 3.** Reflectance of a grating consisted of two dielectric slabs showing validated results.

The frequency dependence for the grating shown in Fig. 3 is given for the spectral range 13–16 GHz. The peak's frequency is exactly 14.9 GHz for the curve in solid line. The following parameters for the curve are used:  $d = 11.28$  mm,  $h = 4.37$  mm,  $\epsilon_{r1} = 6.13$  (Eglass),  $\epsilon_{r2} = 3.7$  (silica), and  $l_1 = l_2 = d/2$ . For these parameters, a half-power bandwidth of 250 MHz is obtained from the range of 14.80–15.05 GHz. The result shows close agreement with that in [10]. Furthermore, the dotted line in the figure depicts resonance at the frequency of 14 GHz, which shows closed agreement with that in [3].

The operating parameters for the dotted lines are:  $\epsilon_{r1} = 2.59$  (Plexiglas),  $\epsilon_{r2} = 2.05$  (Teflon),  $h = 0.7$  cm and  $d = 1.65$  cm. As these results show closed agreements with that obtained by other authors, the validation of our numerical codes is confirmed.

### 3.2. Filter Design

This section is devoted to designing band-stop filters in the microwave frequency region. Firstly, we do parameter checking for single resonance (maximum reflection) at the wanted frequency by changing the size and shape of the elements at normal incidence. For this design process, the goal is to have a more thorough understanding of the relationship of aperture size, shape and periodicity to the spectral response of a DFSS. Deriving some rules from this information would be extremely beneficial to future FSS design work. Unfortunately, from a manufacturing standpoint, it is not always possible to construct an FSS with perfect square apertures. As studying the reflection profile of circular apertures is not enough, one should also investigate the effects of other shapes in controlling reflectance profile like those achieved in this paper.

#### 3.2.1. Choice of Parameters

Since calculation of the reflectance or coupling coefficients for the FSS requires integration over the surface area of an aperture, the resonance wavelengths for the FSSs with equivalent area apertures are

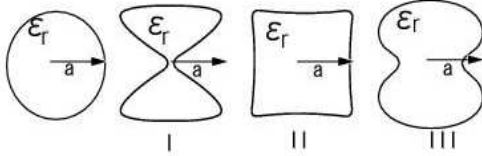


**Figure 4.** Modeling shapes transformation: (I) bowtie, (II) rounded square, (III) deformed elliptical.

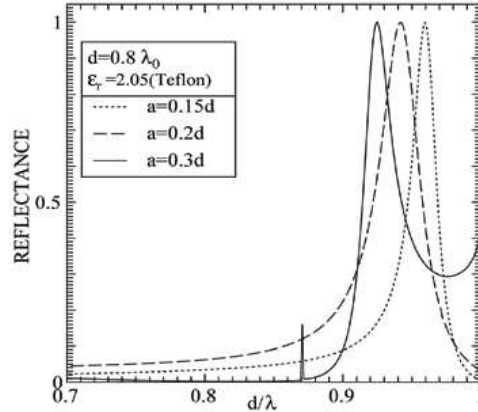


**Figure 5.** Reflectance of a periodic grating showing the effect of cylinder radius for a Teflon grating ( $\epsilon_r = 2.05$ ) with  $d = 0.8\lambda_0$ .

not identical. To understand the variations of the resonance wavelength, we used circular aperture as a base to analyze an arbitrary shaped structures obtained through various transformations, as shown in Fig. 4. In Fig. 4,  $a$  is the radius of the circular cylinder used as the base structure.

The bowtie, rounded square and deformed elliptical shapes are obtained with  $y^4 a^2 \leq x^4(a^2 - x^2)$ ,  $x^4 + 2x^2 a^2 - 2y^2 a^2 + y^4 \leq 0$  and  $(x^2 + y^2 + b^2)^2 \leq 4b^2 x^2 + c^4$ , respectively. The parameters  $b$  and  $c$  are constants that alter the shape of the structure.

We first consider the influence of the aperture size on the reflectance properties for a Teflon grating with  $\epsilon_r = 2.05$  and  $d = 0.8\lambda_0$ , as shown in Fig. 5. It can be seen that the bandwidth and resonance wavelength varies with the aperture size of the cylinder.

A further study is carried out for the influence of the dielectric constant on the reflectance property of the structure. For fixed values of  $a = 0.15d$  and  $d = 0.8\lambda_0$ , the reflectance for several practical available materials is shown in Fig. 6. Our main concern here is to further investigate the bandwidth and reflectance peak shifting effects for the purpose of looking for narrow band filters. Selecting the dielectric constant of the material for design purpose depends on the available materials within the frequency range of interest. From Fig. 6, it can be seen that the reflectance curves for Plexiglas and Polystyrene with relative dielectric constants  $\epsilon_r = 2.59$  and  $\epsilon_r = 2.54$  respectively are very close in profile to each other because of the close material constants. However, it should be pointed out that the resonance wavelength is a nonlinear function of the dielectric contrast between the materials. Fig. 6 also shows that a dielectric material with large constant can lead to broader bandwidth.

This can be explained from resonant waveguide principle that large relative dielectric constant of the grating region leads to an increasing confinement of the modes.

Frequency selective property is also greatly dependent on the shape of the elements in the grating. All results shown here correspond to the shapes in Fig. 4 for  $a = 0.15d$  and  $d = 0.8\lambda_0$  and the reflectance for these shapes is indicated in Fig. 7. The dotted, dashed, solid and dash-dot-dotted lines indicate the result for the circular, the bowtie, the rounded square and the deformed elliptical shape gratings, respectively. It can be seen that rounded square grating shows close reflectance profile to that of a circular cylinder grating with an approximate left-right symmetry because the cross sectional areas are of closed proximity.

Also similar explanation can be given to the bowtie and deformed elliptical shaped gratings that show reflectance profiles close to each other. Since the reflection property depends on the shapes as well as the dielectric constant of the cylinders in the grating, we combined two cylinders with different shapes and material constants in a unit cell for investigation.

When designing a narrowband reflection filter, the array period and the aperture area are clearly the factors that are most important in determining the bandwidth and resonance wavelength. It is also quite apparent that resonance at a specifically desired wavelength requires a very accurately defined period and aperture dimension [20–23].

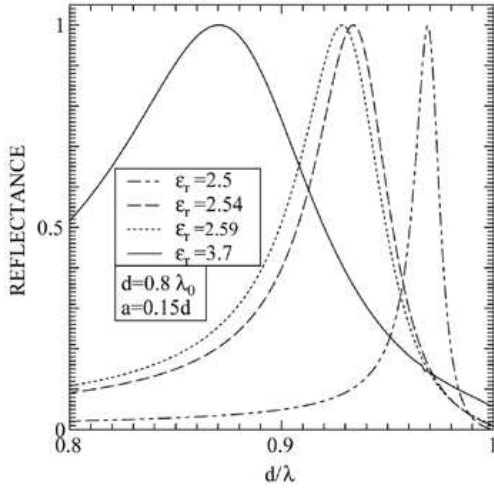


**Figure 6.** Reflectance of a periodic grating showing material effect for a cylinder with  $a = 0.15d$  and  $d = 0.80\lambda_0$ .

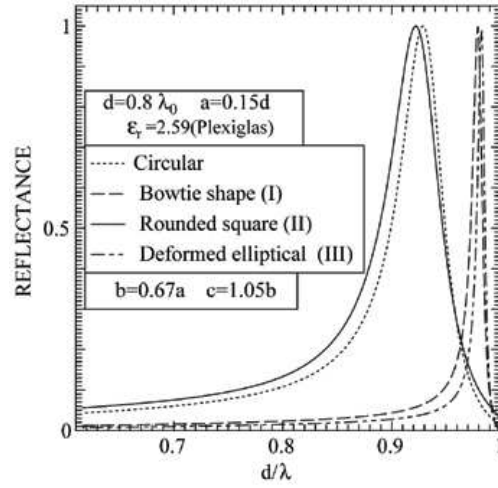


**Figure 7.** Reflectance for various shapes for plexiglass ( $\epsilon_r = 2.59$ ) with  $d = 0.80\lambda_0$ .

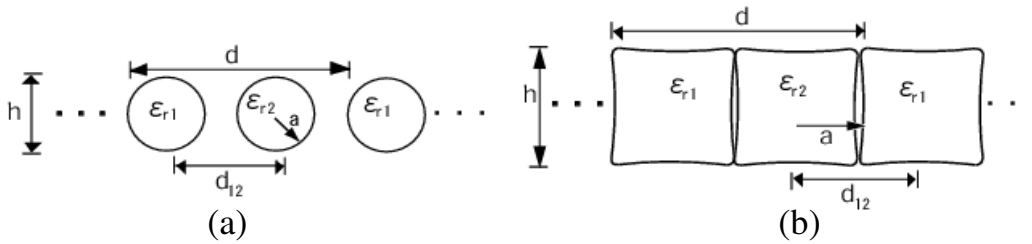


**Figure 8.** (a) Circular aperture grating of radius  $a$ , (b) rounded square aperture. The grating period is denoted by  $d$ , layer thickness  $h = 2a$ , distance between centers  $d_{12}$ , and dielectric constants by  $\epsilon_{r1}$  and  $\epsilon_{r2}$ .

### 3.2.2. Proposed DFSS

Following the analysis in the previous section, several DFSSs consisting of two elements in each unit cell are proposed and studied numerically. It is found after detailed examinations that the shape and suitable dielectric constant strongly affect the resonance peak and bandwidth. However, the circular and rounded square cylinders show possible candidates for the application of narrow band filters and they also show symmetrical line width properties.

In this section, gratings with circular and rounded square apertures, indicated in Fig. 8, are investigated respectively. The two elements in the unit cell are formed by circular cylinders in Fig. 8(a) and by rounded squares in Fig. 8(b) are shown. Both material composition and structural properties such as the distance  $d_{12}$  between cylinders centers can be vary to obtain good filtering properties. The period and thickness are chosen after various numerical calculations in order to set the resonance peak at the center in the frequency band. We examine how  $d_{12}$  affects the bandwidth and resonance frequency of the reflectance profile after setting the resonance peak.

Figure 9 shows how the bandwidth of the filter can be controlled by adjusting the distance between the two apertures in the unit cell. For  $d = 14\text{mm}$ ,  $a = 2.8\text{mm}$ ,  $\epsilon_{r1} = 6.13$  (E-glass), and  $\epsilon_{r2} = 3.7$  (silica), it is possible to design both narrow and broad band filters with the same circular aperture grating as indicated in Fig. 9. For such a design, the half-power bandwidth is broadening as the separation increases. It is also quite evident that a specifically desired resonance wavelength requires accurate period and aperture size prediction. Also, this kind of aperture arrangement shows possible way to control the bandwidth without changing the fundamental parameters.

Generally, as the half-power bandwidth decreases, the resonance frequency becomes more sensitive

with it and a slight shift in it could move peak's frequency away from the spectral band of interest. Fortunately, for the structure discussed and parameters specified, shifting the apertures from  $d_{12} = 0.52d$  to  $0.65d$  has little effect on the peak's frequency as indicated in Fig. 9. This is a useful discovery for the design and applications of DFSS filters.

As a further study, the reflectance for two dielectric materials with  $\epsilon_{r1} = 2.59$  (Plexiglas) and  $\epsilon_{r2} = 2.54$  (Polystyrene) is also investigated, as indicated in Fig. 10 for a circular aperture grating with  $d = 17.6$  mm,  $a = 3.52$  mm and varying  $d_{12}$ . It can be observed from Fig. 10 that the profiles are asymmetrical with both bandwidth and resonance frequency varying simultaneously as the distance between the apertures. This result shows a drastic shift in the peak's frequency as compared to the results shown in Fig. 9. It can be seen that smaller material contrast has stronger effect on the resonance property. In this result, we only concentrate on the effect of altering the distance between apertures for a given period and aperture size, so as to obtain a profile that will lie within the frequency of interest.

The phenomena by the results shown in Figs. 9 and 10 originate from the relative contrast between the two materials and period. However, if the period is small, as for the case in Fig. 9, the relative contrast is the major factor which affects the bandwidth as a result of change in the distribution of materials. If the period is large, the unit cell's structural property would exert an apparent influence, as depicted in Fig. 10.

The reflectance for a rounded square aperture grating is shown in Fig. 11 for which the parameters are:  $d = 16$  mm,  $a = 3.2$  mm, with other parameters being the same as that for Fig. 10. From Fig. 11, it can be seen that a rounded square aperture grating shows a great symmetry property in comparison to that in Fig. 10. In spite of this, increase in distance between cylinders also experiences a negative shift in the resonance frequency, same as observed in Fig. 10 because relative material contrasts are the same.

To find a more precise relationship between  $d_{12}$ , the resonance peaks and bandwidth, more data points from Fig. 11 and Fig. 10 are examined as shown in Fig. 12.

For the bandwidth data, the curves for both circular and rounded square cylinders are given in black circle and blue square marked lines in Fig. 12. The peak frequency curves for both circular and rounded square cylinders are also given in red circle and green square marked lines respectively in Fig. 12. The data shows a slight exponential form indicating the nonlinear relationship between the bandwidth and peak frequency to  $d_{12}$ . The peak frequency experiences a rapid exponential decay for a circular-cylinder grating and a slow exponential decay for a rounded-square cylinder grating. The bandwidth on the other hand shows a slight exponential increase for both circular and rounded-square cylinders.

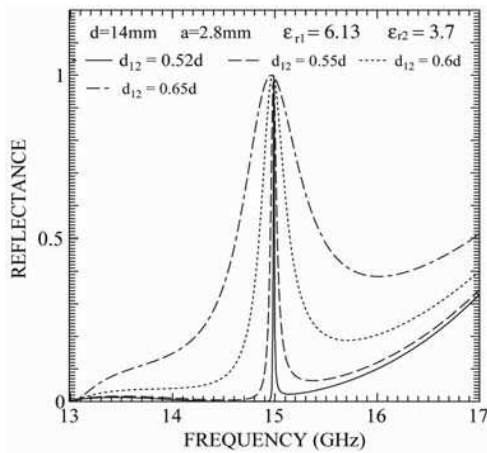


**Figure 9.** Reflectance for a circular aperture grating for the bandwidth controls with relative dielectric constants being the same as that for the solid line in Fig. 3.

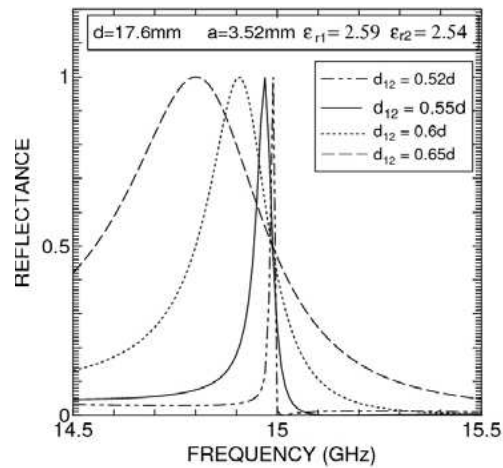


**Figure 10.** Reflectance for a circular aperture grating with  $d = 17.6$  mm,  $a = 3.52$  mm,  $\epsilon_{r1} = 2.59$  (Plexiglas) and  $\epsilon_{r2} = 2.54$  (Polystyrene).

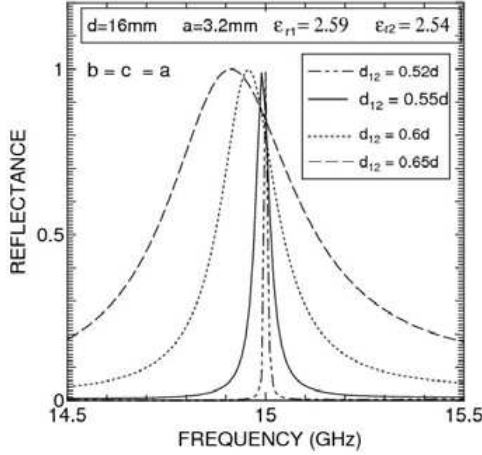


**Figure 11.** Reflectance for a rounded square cylinder grating with  $d = 16$  mm,  $a = 3.2$  mm, and relative dielectric constants the same as that for Fig. 10.

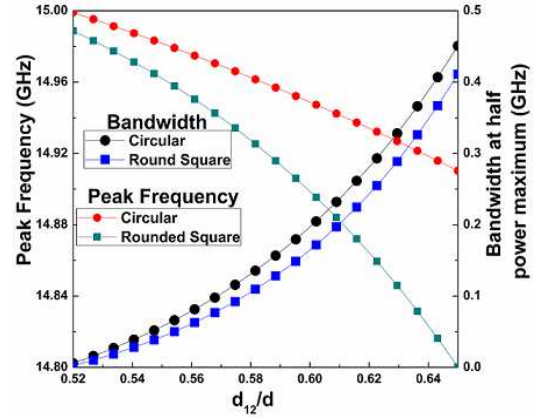


**Figure 12.** Bandwidth and peak frequency versus  $d_{12}$  for both circular and square aperture grating.

It is found that the circular aperture experiences more drift in the resonance (peak) frequency as  $d_{12}$  increases and the bandwidth shows less prominent changes.

### 3.2.3. Influence of Arbitrary Incident Angle on DFSS

Spectral properties for the DFSS at normal incidence have been calculated, and important results are shown in the above sections. For arbitrary incident angles, the electromagnetic field reaches different parts in the array at different times. We will discuss some of their influence on the peak frequency and bandwidth using the parameters in Figs. 9 and 10 for circular elements with results shown in Fig. 13.

The insert between Figs. 13(a) and (c) shows the incidence of plane wave on the unit cell with angle  $\theta$  which is measured from the  $y$ -axis. It can be seen that when an arbitrary angle is incident on the structure, higher Floquet modes are excited. These higher order modes are non-propagation modes that decay exponentially in space. The excitation of these modes gives an unusual spectral property that tends to destroy the resonance peak for normal incidence as shown in Figs. 13(a), (b), (c) and (d). Fig. 13(c) shows that, the first order mode is excited after  $20^\circ$  of incident angle. In Fig. 13(d) it can be seen that, the DFSS acts as a mirror at  $80^\circ$  for a wide range of frequency from 14 GHz to 15.5 GHz. The field patterns clearly show this effect: the field is concentrated above the structure and none below the structure.

### 3.2.4. Application (Narrow-linewidth Filter)

For filter design it is better to use normal incident angle. Further, for line-width filter we use rounded square aperture grating, because its reflectance profiles show symmetry property and experiences less drift in the peak's frequency compared to that of circular aperture structure. It is shown that an FSS with rounded square aperture tends to produce a nice resonance in bandstop reflection profiles. Furthermore, the resonance wavelength and bandwidth appear to be dependent on the periodicity of the array and the dimensions of the apertures.

Figure 14 shows a narrow-linewidth filter for a rounded square cylinder with  $\epsilon_{r1} = 2.59$  (Plexiglas),  $\epsilon_{r2} = 2.54$  (Polystyrene) and  $h = 6.7$  mm. To determine the shape of the rounded square cylinder, the constant  $b = c = 0.67a$  and the radius of the circular cylinder  $a = h/2$  are used. A highly efficient narrow-linewidth filter with a broadly very low sideband reflectance response is realized by careful selection of the structural and material parameters for the grating. A single peak is obtained and the peak frequency is altered by varying the period  $d$ . The two filter lines in Fig. 14 correspond to  $d = 16.1$  mm (solid line) and  $d = 1.5$  mm (dash line), respectively. For the parameters indicated, the peak's frequencies are 13.82 GHz and 14.65 GHz, respectively. The corresponding linewidths (full width

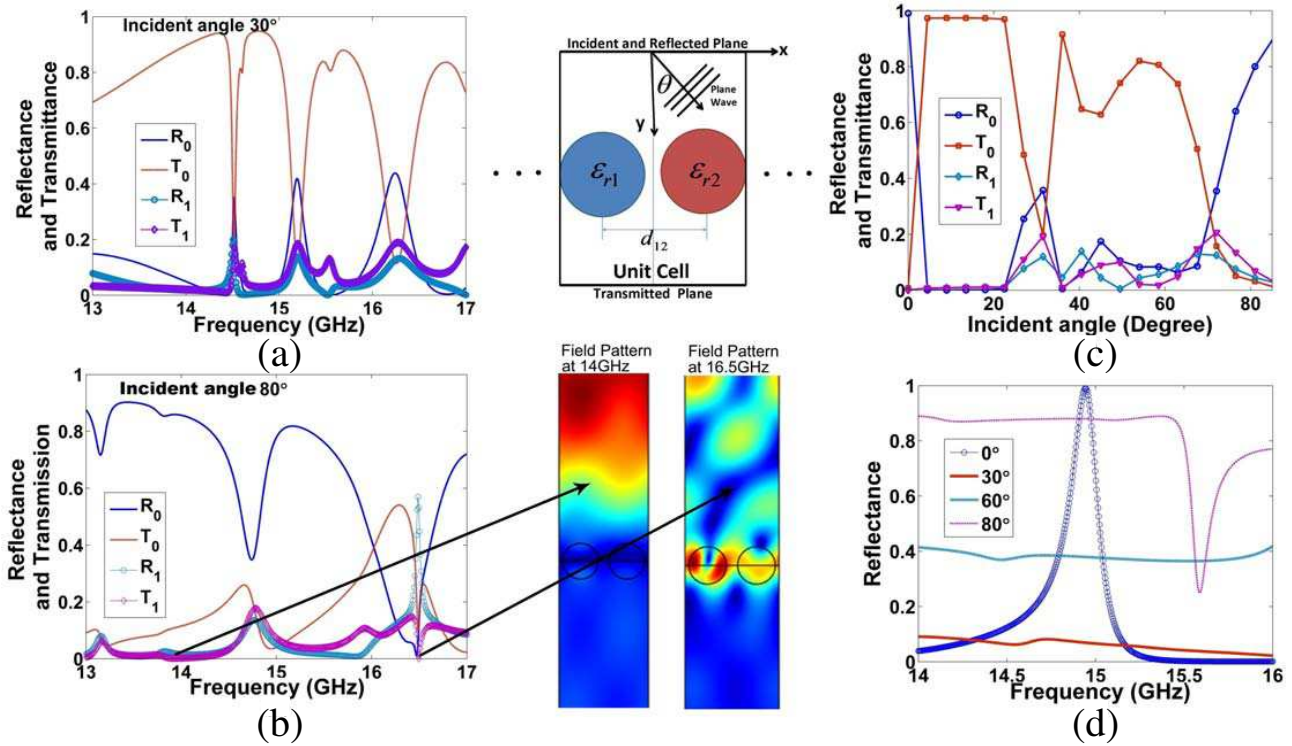


**Figure 13.** Transmittance and reflectance for  $\epsilon_{r1} = 6.13$  (Eglass),  $\epsilon_{r2} = 3.7$  (Silica),  $d = 14\text{mm}$ ,  $a = 2.8\text{mm}$  and  $d_{12} = 0.52d$  with arbitrary incident angle (a)  $\theta = 30^\circ$  and (b)  $\theta = 80^\circ$  (with field patterns shown at 14 GHz and 16.5 GHz); (c) Variation of  $\theta$  at 15 GHz; (d) Reflectance for  $d = 17.6\text{ mm}$ ,  $a = 3.52\text{ mm}$ ,  $\epsilon_{r1} = 2.59$  (Plexiglas),  $\epsilon_{r2} = 2.54$  (Polystyrene) and  $d_{12} = 0.6d$  for various angles of incidence.

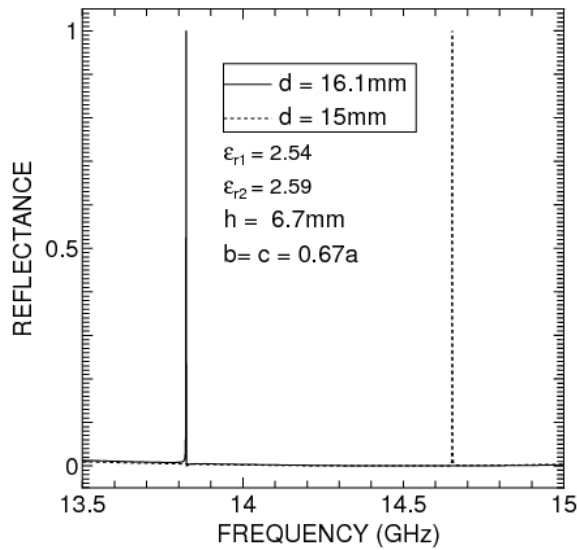


**Figure 14.** Narrow-linewidth filter for a rounded square aperture with  $\epsilon_{r1} = 2.59$  (Plexiglas),  $\epsilon_{r2} = 2.54$  (Polystyrene) and  $h = 6.7\text{ mm}$ .

at half maximum) are 1.48 MHz and 1.43 MHz, respectively. The resulting inter-modulation index is by  $\Delta\varepsilon = \varepsilon_{r2} - \varepsilon_{r1} = 0.05$ .

#### 4. CONCLUSIONS

Frequency selective properties for the periodic array of an arbitrary shaped dielectric cylinder have been numerically examined. It was seen that a DFSS can be designed with specified filtering characteristics, including the peak's frequency, bandwidth reduction, and linewidth control. Using practical materials, a filter design was achieved with peak's frequencies at 13.82 GHz and 14.65 GHz, showing low symmetrical sidebands within the frequency range of interest. The bandwidth of the filter can be controlled by simply adjusting the distance between the two cylinders. Arbitrary incident angles greater  $20^\circ$  can excite higher Floquet modes. Higher incidence angles can destroy the resonance peak as the evanescent modes start propagating. The multilayered frequency selective structure will be proposed in another paper.

#### ACKNOWLEDGMENT

The authors gratefully acknowledge the financial support provided by (i) NSFC (Grant No. 61275043, 61107049, 61171006), (ii) the Guangdong Province NSF (Key project, Grant No. 8251806001000004), and (iii) the Shenzhen Science Bureau (Grant No. 200805, CXB201105050064A).

#### REFERENCES

1. Petit, R., Ed., *Electromagnetic Theory of Grating*, Springer-Verlag, 1980.
2. Yeh, *Optical Waves in Layered Media*, John Wiley & Sons, 1988.
3. Tibuleac, S., R. Magnusson, T. A. Maldonado, P. P. Young, and T. R. Holzheimer, "Dielectric frequency-selective structures incorporating waveguide gratings," *IEEE Trans. on Microwave Theory and Tech.*, Vol. 48, No. 4, 553–561, 2000.
4. Ishimaru, A., *Electromagnetic Wave Propagation, Radiation, and Scattering*, Prentice Hall, 1991.
5. Gerini, G. and L. Zappelli, "Multilayer array antennas with integrated frequency selective surfaces conformal to a circular cylindrical surface," *IEEE Trans. on Antennas and Propagat.*, Vol. 53, No. 6, 2020–2030, 2005.
6. Pelosi, G., A. Cocchi, and A. Monorchio, "A hybrid FEM-based procedure for the scattering from photonic crystals illuminated by a gaussian beam," *IEEE Trans. on Antennas and Propagat.*, Vol. 48, No. 6, 973–980, 2000.
7. Popov, E. and B. Bozhkov, "Differential method applied for photonic crystals," *Appl. Opt.*, Vol. 39, No. 27, 4926–4932, 2000.
8. Koshiba, M., Y. Tsuji, and M. Hikari, "Time-domain beam propagation method and its application to photonic crystal circuits," *J. Lightwave Technol.*, Vol. 18, No. 1, 102–110, 2000.
9. Ikuno, H. and Y. Naka, "Finite-difference time domain method applied to photonic crystals," *Electromagnetic Theory and Applications for Photonic Crystals*, K. Yasumoto, Ed., 401–443, Taylor & Francis, 2006.
10. Coves, A., B. Gimeno, J. Gil, M. V. Andres, A. A. San Blas, and V. E. Boria, "Full-wave analysis of dielectric frequency-selective surfaces using a vectorial modal method," *IEEE Trans. on Antennas and Propagat.*, Vol. 52, No. 8, 2091–2099, 2004.
11. Coves, A., S. Marini, B. Gimeno, and V. Boria, "Full-wave analysis of periodic dielectric frequency-selective surfaces under plane wave excitation," *IEEE Trans. on Antennas and Propagat.*, Vol. 60, No. 6, 2760–2769, 2012.
12. Zappelli, L., "Analysis of modified dielectric frequency selective surfaces under 3-D plane wave excitation using a multimode equivalent network approach," *IEEE Trans. on Antennas and Propagat.*, Vol. 57, No. 4, 1105–1114, 2009.
13. Zappelli, L., "Modified dielectric frequency selective surfaces with enlarged bandwidth and angular stability," *IEEE Trans. on Antennas and Propagat.*, Vol. 59, No. 10, 3668–3678, 2011.

14. Yokota, M. and M. Sesay, "Two-dimensional scattering of a plane wave from a periodic array of dielectric cylinders with arbitrary shape," *J. Opt. Soc. Am. A*, Vol. 25, No. 7, 1691–1696, 2008.
15. Harrington, R., *Field Computation by Moment Methods*, IEEE Press, 1993.
16. Wang, S. S., R. Magnusson, J. S. Bagby, and M. G. Moharam, "Guided-mode resonances in planar dielectric-layer diffraction gratings," *J. Opt. Soc. Am. A*, Vol. 7, No. 8, 1470–1474, 1990.
17. Magnusson, R. and S. S. Wang, "Transmission bandpass guided-mode resonance filters," *Applied Optics*, Vol. 34, No. 35, 8106–8109, 1995.
18. Yasumoto, K. and K. Yoshitomi, "Efficient calculation of lattice sums for free-space periodic Green's function," *IEEE Trans. on Antennas and Propagat.*, Vol. 47, No. 6, 1050–1055, 1999.
19. Lampe, R., P. Klock, and P. Mayes, "Integral transforms useful for the accelerated summation of periodic, free-space Green's functions," *IEEE Trans. on Microwave Theory and Tech.*, Vol. 33, No. 8, 734–736, 1985.
20. Amitay, N., V. Galindo, and C. P. Wu, *Theory and Analysis of Phased Array Antennas*, Wiley-Interscience, New York, 1972.
21. Wu, T. K., Ed., *Frequency Selective Surface and Grid Array*, John Wiley & Sons, New York, 1995.
22. Munk, B. A., R. J. Leubers, and R. D. Fulton, "Transmission through a two-layer array of loaded slots," *IEEE Trans. on Antennas and Propagat.*, Vol. 22, No. 6, 5804–809, 1974.
23. Johansson, F. S., "Analysis and design of double-layered frequency selective surfaces," *IEE Proc.*, Pt. H, Vol. 132, 319–325, 1985.